Magnetic structure and properties of $NaFeSO_4F$ and $NaCoSO_4F$

B. C. Melot,[1] G. Rousse,[2,*] J.-N. Chotard,[1] M. C. Kemei,[3] J. Rodríguez-Carvajal,[4] and J.-M. Tarascon[1]

[1]*Laboratoire de Réactivité et Chimie des Solides, CNRS UMR 6007, Université de Picardie Jules Verne, 33 rue Saint-Leu, F-80039 Amiens, France*

[2]*Institut de Minéralogie et de Physique des Milieux Condensés, UMR 7590, CNRS-Université Pierre et Marie Curie, 4 place Jussieu, F-75252 Paris Cedex 5, France*

[3]*Materials Department and Materials Research Laboratory, University of California, Santa Barbara, California 93106, USA*

[4]*Diffraction Group, Institut Laue-Langevin, 6 rue Jules Horowitz, F-38042 Grenoble Cedex 9, France*

(Received 19 November 2011; published 12 March 2012)

$NaFeSO_4F$ and $NaCoSO_4F$ crystallize in the *maxwellite* crystal structure and consist of one-dimensional chains of corner-sharing MO_4F_2 octahedra linked together through F atoms sitting in a *trans* configuration with respect to each other. Magnetic susceptibility measurements and low-temperature powder neutron diffraction indicate that both the Fe- and Co-based phases establish *G*-type antiferromagnetic ground states below 36 and 29 K, respectively. We discuss the obtained magnetic structure in the context of the local anisotropy of the two magnetic ions.

DOI: 10.1103/PhysRevB.85.094415 PACS number(s): 75.25.−j

I. INTRODUCTION

There has recently been a surge of interest in materials that display electrochemical activity for applications in Li-ion batteries. Besides enabling the transformation of chemical energy into electricity, electrochemically driven redox reactions unlock the ability to tune electronic, ionic, and magnetic properties of 3*d* transition-metal-based inorganic compounds through careful control of oxidation states as well as enabling the preparation of new metastable phases that frequently reveal exotic physical properties. Examples of such properties include superconductivity in $Na_xCoO_2{\cdot}nH_2O$,[1,2] charge ordering in $LiMn_2O_4$,[3–5] and magnetoelectricity in $LiCoPO_4$ and $LiNiPO_4$.[6]

New materials for positive electrodes in Li-ion batteries have recently been discovered with the general formula $AMSO_4F$ (A = Li or Na, M = transition metal), which demonstrates high potentials.[7–10] Despite the vast amount of work devoted to the crystal structure and electrochemical characterization of the recently characterized metastable fluorosulfate phases,[11,12] very little has been done in the way of magnetic characterization with the exception of our earlier report on $LiFeSO_4F$ and $FeSO_4F$, which were shown to order antiferromagnetically at T_N of 25 and 100 K, respectively.[13] With regard to magnetic properties, many of these new phases are potentially very interesting as they consist of a one-dimensional connectivity of the transition-metal polyhedra. Materials with reduced crystallographic dimensionality such as this are extremely attractive as the competition between nearest- and next-nearest-neighbor magnetic exchange interactions often results in a strong interplay between charge, lattice, orbital, and spin degrees of freedom. This competition is well known to give rise to fascinating physical properties such as noncollinear conical spin structures and magnetoelectric coupling.

Aside from the possibility for interesting physics, a detailed understanding of the magnetic structure is absolutely essential for accurate models to be calculated using density functional theory (DFT) codes. Such computational methods have recently provided crucial insight into pathways for sodium and lithium diffusion in fluorosulfates and may eventually give insight into the origin of enhanced redox potentials.[14] Here we present a detailed report of the temperature-dependent magnetic susceptibility for the recently reported fluorosulfate phases $NaFeSO_4F$ and $NaCoSO_4F$.[15] Further, we use low-temperature powder neutron diffraction to propose models for the magnetic structure of both phases.

II. EXPERIMENT

The title compounds were prepared through the dehydration of $NaMSO_4F{\cdot}2H_2O$ in a 1-ethyl-3-methyl imidazolium bis(trifluoromethylsulfonyl)imide (EMI-TFSI) ionic liquid media at 260 °C for several hours. $NaMSO_4F{\cdot}2H_2O$ was prepared via a previously established protocol.[16] Stoichiometric amounts of commercially available $CoSO_4{\cdot}6H_2O$ (or repurified $FeSO_4{\cdot}7H_2O$) and NaF were separately dissolved in enough water to obtain transparent, fully dissolved solutions. The two solutions were then mixed and heated to 80 °C while stirring for approximately 5 h until roughly 90% of the water had evaporated. The product was collected by mixing the resulting solution with a large excess of ethanol, centrifuging, and air drying at 100 °C for 1 h.

Sample purity was analyzed by laboratory powder x-ray diffraction (XRD), using a Bruker D8 diffractometer with Co $K\alpha$ radiation (λ_1 = 1.7892 Å, λ_2 = 1.7932 Å) equipped with a Vantec detector. Neutron-diffraction data were collected either at Institut Laue Langevin (ILL), Grenoble, France, or at Laboratoire Léon Brillouin (LLB), Saclay, France. At ILL, $NaFeSO_4F$ was measured on the D2B and D20 powder diffractometers using wavelengths of 1.594 and 2.420 Å, respectively. The D2B diffractometer has a very high resolution and was therefore used to precisely refine the nuclear structure of $NaFeSO_4F$ at room temperature. The high-intensity powder neutron diffractometer D20, which provides good resolution at low angle, was used to determine the magnetic structure. At LLB, $NaCoSO_4F$ was measured at room temperature and 50 K on the high-resolution 3T2 powder diffractometer using a wavelength of 1.225 Å and on the high-intensity G41 diffractometer with a wavelength of 2.428 Å between 2 and

50 K for the magnetic-scattering part. The FULLPROF suite of programs[17] was used for nuclear and magnetic structure refinements using the Rietveld method[18] as well as bond length and bond-valence-sum calculations.[19] A symmetry analysis was performed using the method of Bertaut[20] as implemented in the BASIREPS[21] program to determine all possible spin configurations that are compatible with the monoclinic symmetry of the title compounds.

The temperature dependence of the dc magnetization was measured on well-ground samples of powder using a Quantum Design magnetic property measurement system (MPMS) 5XL superconducting quantum interference device magnetometer (SQUID).

III. CRYSTAL STRUCTURE

The structures of the title compounds were originally reported to crystallize in a monoclinic $P2_1/c$ space group;[10,22] however, a recent x-ray diffraction study on the NaMSO$_4$F family revealed that $C2/c$ is a more appropriate space group,[15] giving a primitive unit cell with half the volume of the original. Here, using high-resolution powder neutron diffraction, we confirm that the cell does indeed contain a C centering. While neutron diffraction cannot differentiate F and O atoms, given that the scattering factors are so close [$\sigma_{\rm coh}$(F) = 4.017 barns, $\sigma_{\rm coh}$(O) = 4.232 barns], the ability to localize the position of Na atoms is much improved when compared to x-ray scattering.

The room-temperature crystal structures of NaFeSO$_4$F and NaCoSO$_4$F were refined against powder neutron diffraction obtained on D2B and 3T2, respectively, with the results illustrated in Fig. 1. Traces of Na$_3$FeF$_6$ are visible in the neutron-diffraction pattern of NaFeSO$_4$F, so it was included as a secondary phase in the refinement [Fig. 1(a)]. Additionally, the sample of NaCoSO$_4$F was found to have partially reabsorbed water prior to collection of the neutron-diffraction data, which resulted in traces of NaCoSO$_4$F·2H$_2$O, which was therefore included as a secondary phase. The presence of this hydrated phase, together with the high incoherent neutron cross section for cobalt, is a likely origin for the relatively high background observed in Fig. 1(b).

The diffraction patterns of both compounds can be fully indexed to the monoclinic space group $C2/c$. The structures obtained are very similar for the Fe and Co compounds with metal atoms located on the 4a Wyckoff site at the origin of the unit cell and oxygen atoms placed on two 8f sites. Na was found to be on the 4e Wyckoff site, and its atomic displacement parameters were refined anisotropically. A summary of the structural refinement including reliability factors is given in Table I for NaFeSO$_4$F and in Table II for NaCoSO$_4$F. The unit cell volume of the iron-based phase was determined to be 384.344(6) Å^3 versus 374.46(3) Å^3 for the cobalt homologue, as expected for the smaller ionic radius of Co^{2+} [0.745 Å (Ref. 23)] when compared to Fe^{2+} [0.78 Å (Ref. 23)]. A bond-valence-sum analysis (BVS) using the Zachariasen formula [$V_i = \Sigma_j s_{ij} = \Sigma \exp\{(d_0 - d_{ij})/0.37\}$] with the parameter d_0, which characterizes a typical cation-anion distance, taken from Ref. 19, is reported in Tables I and II and shows the good agreement with expected formal charge on each atomic species.

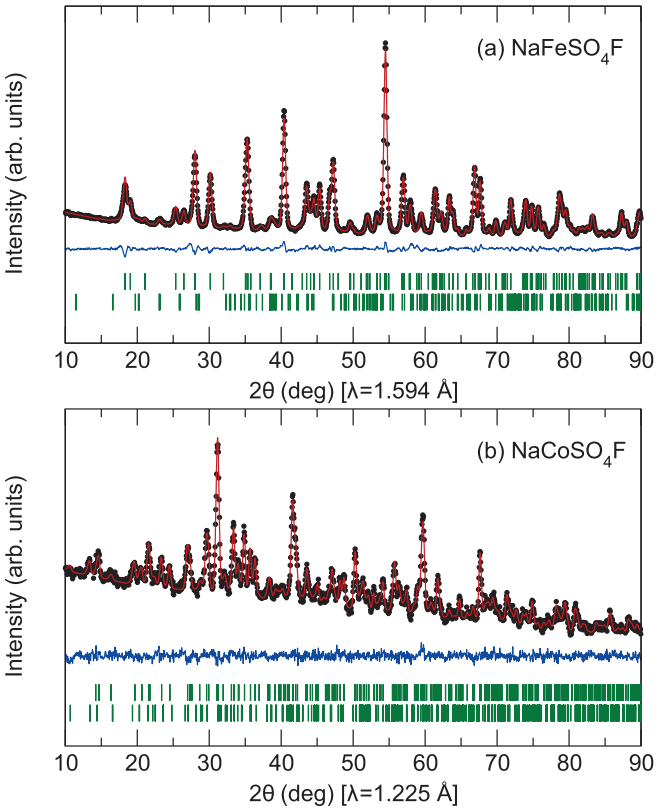

FIG. 1. (Color online) Portion of the refined powder neutron-diffraction patterns (observed shown as black circles, and calculated shown as the red line) at room temperature for (a) NaFeSO$_4$F collected on D2B (λ = 1.594 Å) at the ILL and (b) NaCoSO$_4$F collected on 3T2 (λ = 1.225 Å) at the LLB. The positions of the Bragg reflections are shown as vertical bars below. [The first line shows NaFeSO$_4$F (a) or NaCoSO$_4$F (b). The second line of ticks marks corresponds to 6 wt % Na$_3$FeF$_6$ impurity (a) and 1 wt % NaCoSO$_4$F·2H$_2$O (b).] Note the higher background level for (b) due to the high incoherent scattering length of cobalt and hydrogen from the hydrated impurity. The difference (observed minus calculated) line is displayed in blue.

The crystal structure of NaFeSO$_4$F and NaCoSO$_4$F is illustrated in Fig. 2. Apart from the small volume change, both compounds are isostructural and show no evidence of changes in the nuclear symmetry on cooling aside from the effects expected from thermal contraction. They are composed of MO$_4$F$_2$ octahedra that are bound together at their corners through F atoms, which are oriented in a *trans* configuration with respect to each other, giving rise to buckled chains. All of the oxygen atoms in the structure are bound within SO$_4$ tetrahedra, which connect the chains via shared corners on the MO$_4$F$_2$ octahedra. These chains, which run along the c axis of the unit cell, are illustrated in Figs. 2(a) and 2(b). Na sits in channels that run along the [110] and [1$\bar{1}$0] directions and is coordinated to four oxygen and one fluorine at distances ranging from 2.2 to 2.5 Å. It should also be noted that there is only one unique M site in both structures and that the M-F-M bond angle dictates the degree of buckling along the chains.

TABLE I. Crystallographic data and atomic positions of $NaFeSO_4F$ resulting from refinements of the structure against the data collected on the high-resolution powder neutron diffractometer D2B (ILL, Grenoble, France) obtained at room-temperature $R_{\text{Bragg}} = 2.81\%$, $\chi^2 = 3.86$. Results from the BVS are also indicated.

Space group			$C2/c$			
a (Å)			6.68655(7)			
b (Å)			8.71252(8)			
c (Å)			7.19527(7)			
α (°)			90			
β (°)			113.5213(8)			
γ (°)			90			
V (Å^3)			384.344(6)			
Atom	Wyckoff	x	y	z	B_{iso}(Å^2)	BVS
Na	4e	0	0.3371(4)	$\frac{1}{4}$	anisotropic[a]	0.93(1)
Fe	4a	0	0	0	0.55(2)	2.04(1)
S	4e	0	0.6789(4)	$\frac{1}{4}$	0.68(7)	6.00(1)
O1	8f	0.6068(2)	0.2778(2)	0.1483(2)	0.95(2)	1.91(1)
O2	8f	0.3387(2)	0.0810(2)	0.0985(2)	0.95(2)	2.01(1)
F	4e	0	0.0856(3)	$\frac{1}{4}$	0.97(3)	1.14(1)

[a]Anisotropic β ($\times 10^4$): $\beta_{11} = 151(11)$, $\beta_{22} = 14(5)$, $\beta_{33} = 377(16)$, $\beta_{12} = 0$, $\beta_{13} = 61(11)$, $\beta_{23} = 0$.

IV. MAGNETIC SUSCEPTIBILITY

The temperature dependence of the magnetic susceptibility for both phases is shown in Fig. 3, where cusps indicative of long-range antiferromagnetic order can be seen at 36 K for $NaFeSO_4F$ and 29 K for $NaCoSO_4F$. A minimum field of 10 kOe was necessary to suppress the contribution from the magnetic impurity phases discussed above; however, the presence of these phases can still be seen in the paramagnetic tail that occurs after the bulk magnetic transition temperature. There is a significant difference in the sharpness of this peak between the cobalt- and iron-based phases.

The high-temperature region (200–300 K) of the susceptibility was fit to a modified Curie-Weiss equation, $\chi = C/(T - \Theta_{CW}) + \chi_0$, which includes a temperature-independent term to account for the background contribution of the impurity phases. The resulting fit to the data for $NaFeSO_4F$ gave an effective paramagnetic moment of 5.40 μ_B per Fe, Θ_{CW} of -104 K, and $\chi_0 = -6.8 \times 10^{-4}$ emu mol^{-1} Oe^{-1}. Such an effective moment matches well to the 5.48 μ_B that is expected for a high-spin Fe^{2+} ion (d^6, $t_{2g}^4 e_g^2$, $S = 2, L = 2$) with an unquenched orbital moment that is fully decoupled from the spin contribution as calculated using the equation $\mu_{L+S} = \sqrt{4S(S+1) + L(L+1)}$.[24]

Fits to the $NaCoSO_4F$ data gave an effective paramagnetic moment of 5.20 μ_B per Co, Θ_{CW} of -72 K, and $\chi_0 = -4.2 \times 10^{-4}$ emu mol^{-1} Oe^{-1}. In this case, the effective moment is also in perfect agreement with the 5.20 μ_B expected

TABLE II. Crystallographic data and atomic positions of $NaCoSO_4F$ resulting from refinements of the structure against the data collected on the high-resolution powder neutron diffractometer 3T2 (LLB, Saclay, France) obtained at room-temperature $R_{\text{Bragg}} = 2.62\%$, $\chi^2 = 1.10$. Results from the BVS are also indicated.

Space group			$C2/c$			
a (Å)			6.6687(4)			
b (Å)			8.6251(5)			
c (Å)			7.1444(4)			
α (°)			90			
β (°)			114.323(3)			
γ (°)			90			
V (Å^3)			374.46(3)			
Atom	Wyckoff	x	y	z	B_{iso}(Å^2)	BVS
Na	4e	0	0.331(1)	$\frac{1}{4}$	anisotropic[a]	0.99(1)
Co	4a	0	0	0	1.51(28)	2.08(1)
S	4e	0	0.680(1)	$\frac{1}{4}$	0.19(20)	5.72(6)
O1	8f	0.6067(6)	0.2797(4)	0.1454(6)	1.13(3)	1.88(3)
O2	8f	0.3335(5)	0.0788(5)	0.0950(5)	1.13(3)	1.91(3)
F	4e	0	0.0852(9)	$\frac{1}{4}$	1.13(3)	1.21(1)

[a]Anisotropic β ($\times 10^4$): $\beta_{11} = 185(34)$, $\beta_{22} = 15(4)$, $\beta_{33} = 233(38)$, $\beta_{12} = 0$, $\beta_{13} = 5(33)$, $\beta_{23} = 0$.

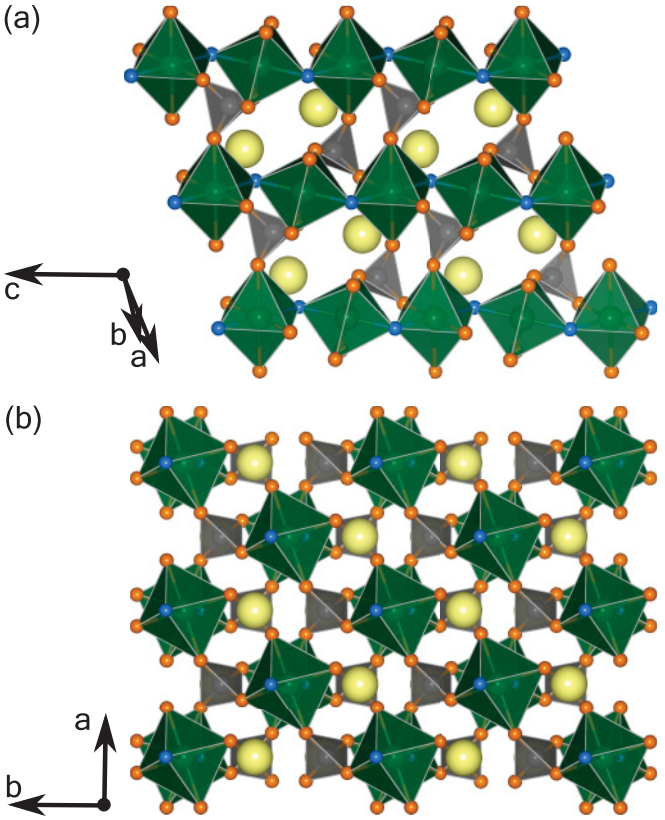

FIG. 2. (Color online) (a) Illustration of the crystal structure of $NaFeSO_4F$ and $NaCoSO_4F$ perpendicular to the $[\bar{1}10]$ direction, showing the "tavorite cages." Co or Fe atoms sit in the middle of the green octahedra, SO_4 tetrahedra are grey, and Na and O atoms are displayed as large yellow and small orange balls, respectively. (b) Illustration of the crystal structure perpendicular to the c axis of the monoclinic $C2/c$ cell. The structure is composed of corner-sharing octahedra, which share corners through F atoms (in blue) sitting *trans* with respect to each other along the length of the chains.

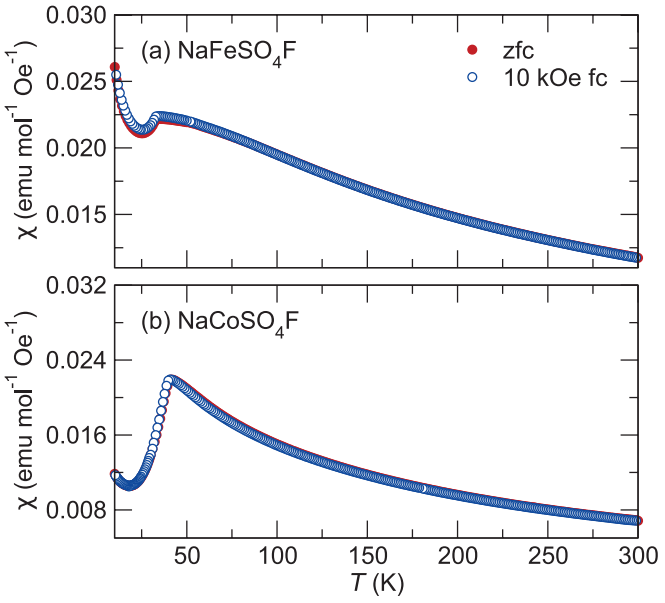

FIG. 3. (Color online) Temperature-dependent magnetic susceptibility of (a) $NaFeSO_4F$ and (b) $NaCoSO_4F$ collected in a field of 10 kOe.

for a high-spin Co^{2+} ion (d^7, $t_{2g}^5 e_g^2$, $S = 3/2, L = 3$) with an unquenched orbital moment that is fully decoupled from the spin contribution. The negative sign on both Θ_{CW} confirms that the dominant magnetic superexchange is antiferromagnetic, as seen in the rapid downturn of the susceptibility with the onset of magnetic order.

V. POWDER NEUTRON DIFFRACTION

Neutron-diffraction patterns were collected between 2 and 60 K for $NaFeSO_4F$ on the high-intensity D20 powder diffractometer at ILL and between 2 and 50 K for $NaCoSO_4F$ on the high-intensity powder neutron diffractometer G41 at the LLB. Both instruments are especially well adapted for magnetic structure determination, using a wavelength of 2.42 Å with good resolution at low 2θ angles.

Below the respective ordering temperature several new peaks corresponding to the onset of long-range magnetic ordering begin to evolve. The intensity of the strongest magnetic reflection for both phases is plotted as a function of temperature in Fig. 4(a), with the observed ordering temperature in good agreement with the temperature-dependent susceptibility data. As the structures are identical, the reduced magnetic ordering temperature for the Co^{2+} analog (T_N = 29 K) as compared to Fe^{2+} (T_N = 36 K) is expected to be due to the increased occupancy of the antibonding levels and is in good agreement with what is typically observed. Note that the increased ordering temperature with respect to the tavorite phase $LiFeSO_4F$ (25 K) can be explained by the increased Fe-F-Fe angle [129.3° in $LiFeSO_4F$ (Ref. 13) compared to 134.9° for $NaFeSO_4F$] approaching the ideal angle of 180°, in agreement with the general theory of superexchange.[25–27]

VI. RESULTS AND DISCUSSION

Figures 4(b) and 4(c) illustrate the new magnetic peaks that evolve below the ordering temperature. The magnetic reflections for both compounds can be indexed with a propagation vector $\mathbf{k} = (1,0,0)$, so that the C centering of the lattice is broken with the onset of magnetic order. The little group $G_{\mathbf{k}}$ coincides with the full $G = C2/c$ space group because all of the operators of G leave the propagation vector $\mathbf{k} = (1,0,0)$ invariant (up to a reciprocal lattice vector). There are two one-dimensional irreducible representations associated with the $4a$ site where the metal sits: $\Gamma_{\text{mag}} = 3\Gamma_1 \oplus 3\Gamma_3$. Each representation is composed of three basis vectors that correspond to moments oriented along the a, b, or c unit-cell directions, as given in Table III. The basis vectors of the Γ_1 representation correspond to a coupling where the two metal atoms within a primitive cell, located at 1: (0,0,0) and 2: $(0,0,\frac{1}{2})$ in the conventional cell, are oriented parallel along b and antiparallel along a and c. The magnetic moments are of the form (u,v,w) and $(-u,v,-w)$, respectively. In contrast, the basis vectors of the Γ_3 representation correspond to the coupling (u,v,w) and $(u,-v,w)$. The rest of magnetic moments in the crystal can be obtained from the magnetic

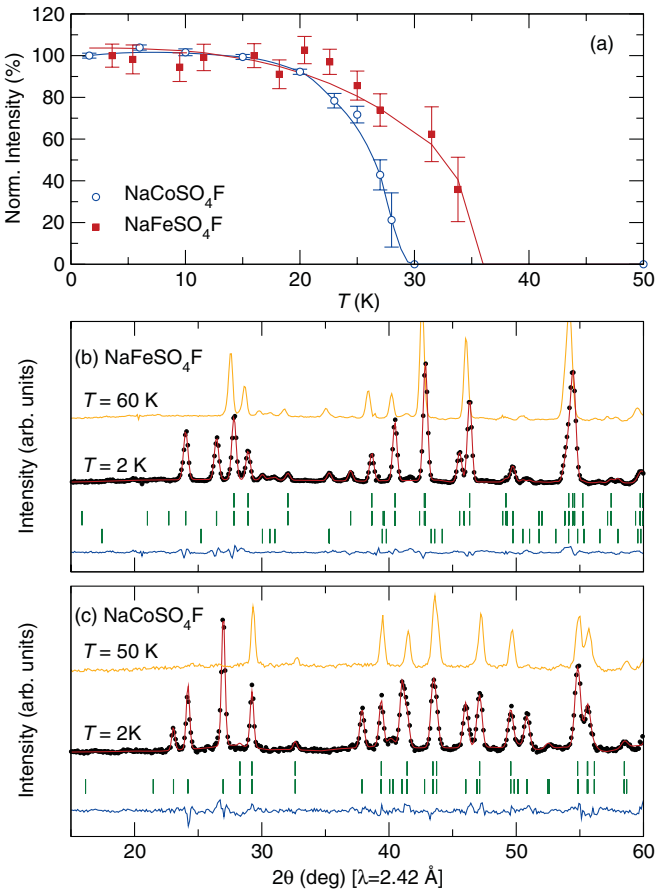

FIG. 4. (Color online) Neutron powder diffraction on title compounds. (a) Evolution of intensity of the main magnetic peak with temperature. For $NaFeSO_4F$ (red squares), the magnetic reflection is $(\bar{1}01)$ at $2\theta = 24.02^\circ$, and for $NaCoSO_4F$ (blue circles), the magnetic peak is the $(0\bar{1}1)/(011)$ at $2\theta = 26.97^\circ$. Lines are a guide for the eyes. Note that the ordering temperatures are in good agreement with the temperature-dependent susceptibility. Magnetic Rietveld refinement of the title compounds: Observed (black dots) vs calculated (red line) powder neutron diffraction patterns of (b) $NaFeSO_4F$ on D20 with $\lambda = 2.42$ Å and (c) $NaCoSO_4F$ on G41 (LLB) with $\lambda = 2.42$ Å collected at 2 K. The difference pattern (blue line) is displayed at the bottom of each panel. The patterns recorded above the magnetic transition are displayed (orange line) for comparison at 60 K for $NaFeSO_4F$ and 50 K for $NaCoSO_4F$. The positions of the Bragg reflections are shown as vertical bars below. [For $NaFeSO_4F$ in (b), the first line is nuclear, the second line is magnetic, and third line is the Na_3FeF_6 impurity. For $NaCoSO_4F$ in (c) the first line is nuclear, and the second line is magnetic.]

moments of the sublattice $j(1, 2)$ in the zero cell with the expression

$$\begin{aligned}\mathbf{m}_{lj} &= \mathbf{m}_{0j}\exp\{-2\pi i\mathbf{k}\mathbf{R}_l\}\\ &= \mathbf{m}_{0j}\exp\{-2\pi i(1\mathbf{a}^*)(l_1\mathbf{a}+l_2\mathbf{b}+l_3\mathbf{c})\}\\ &= \mathbf{m}_{0j}\exp\{-2\pi i l_1\} \qquad (1)\end{aligned}$$

where the lattice translation $\mathbf{R}_l = l_1\mathbf{a} + l_2\mathbf{b} + l_3\mathbf{c}$ contains integer values as well as rational values due to the centering translation $\mathbf{t}_C = (\frac{1}{2},\frac{1}{2},0)$; for instance, the $(\frac{1}{2},\frac{1}{2},0)$ set of atoms in the conventional cell has its moment opposite to those of the zero cell because $\exp(-2\pi i\, l_1) = \exp(-2\pi i\frac{1}{2}) = -1$. The two possible configurations were tested, and it was found that the best agreement with the observed magnetic reflections is obtained when $\Gamma_1\{\mathbf{m}_{01} = (u,v,w),\ \mathbf{m}_{02} = (-u,v,-w)\}$ is used for both of the title compounds; however, there are significant differences between the two magnetic structures due to different values of the (u,v,w) components. For $NaFeSO_4F$, the magnetic moment on each Fe^{2+} has a nearly zero v component, so the moments are within the ac plane. The results of the Rietveld refinement give moments that primarily point along c with a contribution along a: $\mathbf{m}_{01,Fe} \approx (u,0,w)$. The magnitude of the magnetic moment is 3.85(4) μ_B, in agreement with values typically observed for octahedrally coordinated Fe^{2+}.[28–30] In contrast, while the main component of the magnetic moment in $NaCoSO_4F$ is also oriented along the c axis, the nearly zero component is along the a axis, with the minor component oriented along the b axis: $\mathbf{m}_{01,Co} \approx (0,v,w)$. The magnetic moment for Co^{2+} refines to a value of 4.06(4) μ_B, which is higher than the value of 3.0 expected for the spin-only contribution from a high-spin octahedrally coordinated d^7 ion. Such a result is a reflection of the unquenched orbital contribution to the magnetic moment that was identified in the Curie-Weiss analysis of the temperature-dependent magnetic susceptibility data and is in good agreement with what has typically been seen for Co^{2+} ions.[31–33]

The resulting magnetic structures of $NaFeSO_4F$ and $NaCoSO_4F$ are gathered in Table IV and illustrated in Fig. 5. In both compounds, the moments are oriented antiparallel along the length of the chains as well as between the chains. If we consider the chains of MO_4F_2 as having a perovskite-like topology, then the magnetic structures of $NaFeSO_4F$ and $NaCoSO_4F$ may be described using the notation developed by Wollan and Koehler.[34] Applying this nomenclature to the four atoms within the conventional cell, numbered in the order 1: (0,0,0), 2: $(0,0,\frac{1}{2})$, 3: $(\frac{1}{2},\frac{1}{2},\frac{1}{2})$, and 4: $(\frac{1}{2},\frac{1}{2},0)$, and considering only the c component, both compounds adopt a magnetic structure analogous to a G-type $(+,-,+,-)$ antiferromagnetic structure where all the spins on nearest-neighbor magnetic ions are antiferromagnetically aligned. Within this nomenclature the magnetic structure of $NaFeSO_4F$ can be labeled as $(G_x,0,G_z)$, a pure G mode, whereas that of $NaCoSO_4F$ can be labeled as $(0,C_y,G_z)$.

TABLE III. Representation analysis for the magnetic structure. The basis functions for the two possible representations, Γ1 and Γ3, are indicated. How the magnetic moments on the two metal atoms related with the symmetry operation $-x,y,-z+\frac{1}{2}$ of space group $C2/c$ are related by symmetry when the magnetic propagation vector is $\mathbf{k} = (1,0,0)$ is also indicated.

Basis vectors representation	M(Co/Fe) in (000)	M(Co/Fe) in $(00\frac{1}{2})$
Γ_1	(100)	$(\bar{1}00)$
	(010)	(010)
	(001)	$(00\bar{1})$
Γ_3	(100)	(100)
	(010)	$(0\bar{1}0)$
	(001)	(001)

TABLE IV. Magnetic structure of $NaFeSO_4F$ and $NaCoSO_4F$ determined from refinement of the structure against powder neutron diffraction on D20, ILL, at 2 K ($NaFeSO_4F$) or on G41, LLB, at 2 K ($NaCoSO_4F$). All the magnetic atoms in the conventional cell are given with the components listed along a,b,c in μ_B and were determined using Γ_1.

		$NaFeSO_4F$[a]		
Atom	m_a	m_b	m_c	M_{Total} (μ_B)
Fe(000)	1.427(55)	0	4.187(39)	3.847(37)
Fe(00$\frac{1}{2}$)	−1.427(55)	0	−4.187(39)	3.847(37)
Fe($\frac{1}{2}\frac{1}{2}\frac{1}{2}$)	1.427(55)	0	4.187(39)	3.847(37)
Fe($\frac{1}{2}\frac{1}{2}$0)	−1.427(55)	0	−4.187(39)	3.847(37)
		$NaCoSO_4F$[b]		
Atom	m_a	m_b	m_c	M_{Total} (μ_B)
Co(000)	0	1.270(47)	3.860(40)	4.063(45)
Co(00$\frac{1}{2}$)	0	1.270(47)	−3.860(40)	4.063(45)
Co($\frac{1}{2}\frac{1}{2}\frac{1}{2}$)	0	−1.270(47)	3.860(40)	4.063(45)
Co($\frac{1}{2}\frac{1}{2}$0)	0	−1.270(47)	−3.860(40)	4.063(45)

[a] $R_{\text{mag}} = 9.09\%$, propagation vector $\mathbf{k} = (1,0,0)$, magnetic mode $(G_x,0,G_z)$.
[b] $R_{\text{mag}} = 8.10\%$, propagation vector $\mathbf{k} = (1,0,0)$, magnetic mode $(0,C_y,G_z)$.

While the magnetic structures of both compounds are similar with respect to the main spin sequence along the c axis, the absolute orientation of the moments presents some interesting differences. The main component of the magnetic moment in both phases is along c, but the secondary component orients along the a axis in $NaFeSO_4F$ and along the b axis in $NaCoSO_4F$. One can see from Fig. 5 that while the pure G mode results in a collinear magnetic structure in the case of the Fe-based phase, the mixed mode $(0,C_y,G_z)$ in the Co-based phase results in a noncollinear structure with magnetic moment tilted in alternative sequence along c toward one side or the other of the b axis. Moreover, the moments in the Co-based phase are oriented such as they point toward apexes of the octahedra where the F atoms sit such that they are parallel to the quasifourfold pseudosymmetry axis of rotation. In contrast, the moments in $NaFeSO_4F$ are oriented almost perpendicular to the (a, b) plane. Such an orientation is a reflection of the strong magnetocrystalline anisotropy of the Co^{2+} ion, which results from the relatively strong spin-orbit coupling, which is a common feature in Co-based phases and has been observed in several other cobalt-containing compounds.[35,36] It should also be noted that we have previously encountered a similar anisotropic orientation of the magnetic moments in the tavorite phase of $LiFeSO_4F$[13] of the fluorosulfate family where the spins on the orbitally degenerate Fe^{2+} ions align along the local pseudosymmetry axis.

Inspection of the neutron-diffraction patterns as a function of temperature shows that no additional magnetic reflections develop below the onset of long-range order. An analysis of the relative strengths and signs of the different exchange interactions in the structures required to produce the observed magnetic structure has been done. It should be noted that this analysis neglects the magnetocrystalline anisotropy, which plays a role in $NaFeSO_4F$ and $NaCoSO_4F$. We follow here using a procedure similar to that applied to other polyanionic iron compounds.[28–30,37,38]

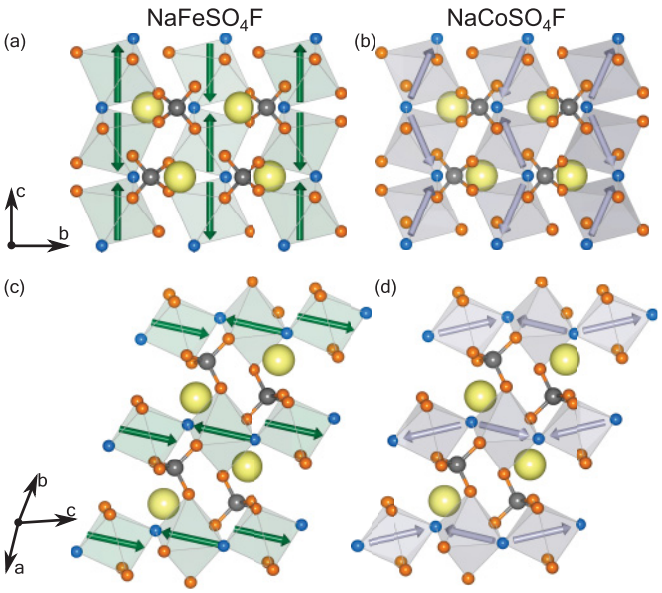

FIG. 5. (Color online) Illustration of the proposed magnetic structures of (a),(c) $NaFeSO_4F$ and (b),(d) $NaCoSO_4F$. Magnetic moments on the Fe^{2+} or Co^{2+} ions are indicated with arrows. The color code is the same as in Fig. 2. The moments along the length of the chains are aligned antiparallel, and the chains are also coupled antiparallel, giving a G-type antiferromagnetic structure.

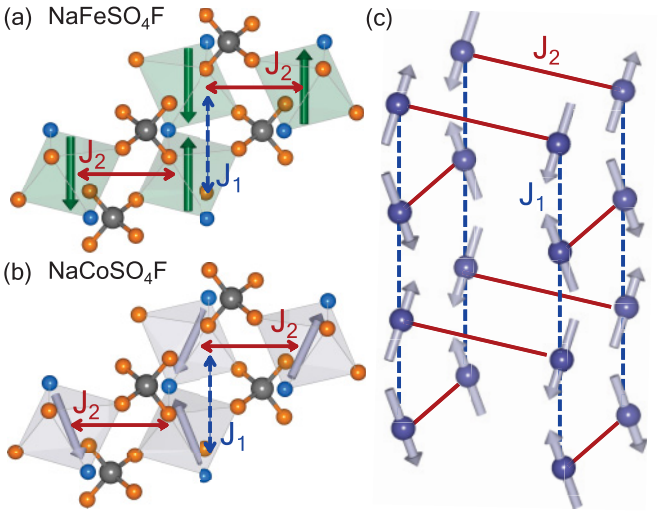

FIG. 6. (Color online) Illustration of the superexchange and supersuperexchange pathways considered in (a) $NaFeSO_4F$ and (b) $NaCoSO_4F$. Fluorine atoms are blue, oxygen atoms are orange, and sulfur atoms are grey. J_1 is the exchange pathway between neighboring metal atoms within the chains mediated via an F atom (superexchange) or via SO_4 tetrahedron (supersuperexchange). J_2 connects metal atoms in adjacent chains through a supersuperexchange pathway, which is doubly degenerate with two distinct SO_4 tetrahedra linking neighbors. (c) Illustration of the topology of the exchange pathways considered here. Orientation of moments corresponds here to the cobalt analog. Note that from this topology it is clear that there is no geometrical frustration present.

TABLE V. List of exchange paths and their geometrical characteristics for $NaFeSO_4F$ and $NaCoSO_4F$. S denotes a superexchange interaction, while SS indicates a supersuperexchange pathway.

	$NaFeSO_4F$			
	J_1		J_2	
Direct Fe-Fe distance	3.598 Å (intrachain)		5.491 Å (interchain)	
Path type	S (via F)	SS	SS	SS
Fe–O (Å)	1.947	2.188	2.188	2.202
O–O (Å)	–	2.418	2.402	2.402
O–Fe (Å)	1.947	2.188	2.202	2.188
Fe–O–O (°)	–	97.9	118.7	152.5
O–O–Fe (°)	–	97.9	152.5	118.7
Torsion angle (°)	134.9	−53.4	13.8	−13.8
	$NaCoSO_4F$			
	J_1		J_2	
Direct Co–Co distance	3.578 Å (intrachain)		5.459 Å (interchain)	
Path type	S (via F)	SS	SS	SS
Co–O (Å)	1.938	2.141	2.141	2.150
O–O (Å)	–	2.473	2.447	2.447
O–Co (Å)	1.938	2.141	2.150	2.141
Co–O–O (°)	–	97.4	118.4	152.6
O–O–Co (°)	–	97.4	152.6	118.4
Torsion angle (°)	134.7	−53.4	15.4	−15.4

The first ordered state is obtained by a calculation as a function of $\mathbf{k}$ (on the surface or at the interior of the Brillouin zone) and the exchange integrals. This state is given by the eigenvector corresponding to the highest eigenvalue (giving the highest transition temperature, $\lambda_{\max} = 3k_BT$) of the Fourier transform of the exchange integral matrix:

$$\xi_{ij}(\mathbf{k}) = \sum_l J_{ij}(\mathbf{R_l}) e^{-2\pi i \mathbf{k}\mathbf{R_l}}, \tag{2}$$

where i and j refer to the magnetic atoms in a primitive cell and $J_{ij}(\mathbf{R}_l)$ is the isotropic exchange interaction between the spins of atoms i and j in unit cells separated by the lattice vector $\mathbf{R}_l$. Our convention is that negative J_{ij} means antiparallel coupling (pair interaction energy: $E_{ij} = -J_{ij}\,\mathbf{S}_i\mathbf{S}_j$). Examination of the exchange pathway in both compounds shows that the principal magnetic exchange interaction between nearest-neighbor ions, denoted as J_1 in Figs. 6(a)–6(c), occurs either through a superexchange path M-F-M linkage along the length of the chain or else through M-O-O-M supersuperexchange pathways along the edge of the SO_4 tetrahedra. In contrast, the next-nearest-neighbor interactions are entirely mediated by supersuperexchange interactions along the edge of the SO_4 tetrahedra, which are doubly degenerate and are labeled as J_2 in Figs. 6(a)–6(c). A third supersuperexchange interaction also exists between metal ions in the adjacent chains; however, since this pathway only involves a single SO_4 group, it is reasonable to consider this interaction will be negligible when compared with the strength of J_1 and J_2. Table V lists the geometric characteristics of the two exchange paths J_1 and J_2. The bond distances and angles are similar for both title compounds, except the longer bonds for the Fe-based phase, in agreement with the larger ionic radius.

The phase diagram is easily obtained using the programs SIMBO and ENERMAG[39] or by hand determining the eigenvalues and eigenvectors of the matrix:

$$\xi(\mathbf{k}, J_1, J_2) = \begin{pmatrix} 2J_2 \cos\pi(k_x + k_y) & J_1(1 + e^{2\pi i k_z}) \\ J_1(1 + e^{2\pi i k_z}) & 2J_2 \cos\pi(k_x - k_y) \end{pmatrix}. \tag{3}$$

The phase diagram is very simple (except for singular points with no order, null J_1 or J_2, or isolated points): when J_2 is positive, the propagation vector is $\mathbf{k} = (0,0,0)$, and if J_2 is negative, $\mathbf{k} = (1,0,0)$. In our case the observed propagation vector is $\mathbf{k} = (1,0,0)$, so J_2 must be negative. The sign of J_1 determines the coupling mode between the atoms 1: (0,0,0) and 2: $(0,0,\frac{1}{2})$ (relative sign of the eigenvectors). If J_1 is positive, the mode is $(+,+)$, which corresponds to the C mode if the four atoms of the conventional cell are considered in the case of $\mathbf{k} = (1,0,0)$ and to an F mode for $\mathbf{k} = (0,0,0)$. If J_1 is negative, the mode is $(+,-)$, which corresponds to the G mode in the case of $\mathbf{k} = (1,0,0)$ and to an A mode for $\mathbf{k} = (0,0,0)$. The observed magnetic structures easily lead to negative values of J_1 and J_2 for both compounds.

VII. CONCLUSIONS

We have presented a detailed report on the temperature-dependent magnetic susceptibility for two recently reported fluorosulfate phases, $NaFeSO_4F$ and $NaCoSO_4F$. We have furthermore used low-temperature powder neutron diffraction to propose models for the magnetic structure of both phases and analyzed the structure in terms of the local anisotropy of the constituent ions. It is our hope that this information on the magnetic structure will encourage computational efforts to more carefully examine the effect of the structure on the accuracy of DFT calculations.

ACKNOWLEDGMENTS

We would like to thank Mohamed Ati for assisting with the preparation of samples and for fruitful discussions, Gilles André and Florence Porcher for measuring our samples at LLB, and Michella Brunelli for her help during neutron-diffraction experiments at ILL. M.C.K. is supported by the Schlumberger Foundation Faculty for the Future Fellowship and the NSF Materials World Network grant. We acknowledge the use of shared experimental facilities of the Materials Research Laboratory.

*gwenaelle.rousse@upmc.fr

[1] R. E. Schaak, T. Klimczuk, M. L. Foo, and R. J. Cava, Nature (London) **424**, 527 (2003).

[2] J. M. Tarascon, G. Vaughan, Y. Chabre, L. Seguin, M. Anne, P. Strobel, and G. Amatucci, J. Solid State Chem. **147**, 410 (1999).

[3] J. Rodríguez-Carvajal, G. Rousse, C. Masquelier, and M. Hervieu, Phys. Rev. Lett. **81**, 4660 (1998).

[4] G. Rousse, C. Masquelier, J. Rodriguez-Carvajal, and M. Hervieu, Electrochem. Solid State Lett. **2**, 6 (1999).

[5]G. Rousse, C. Masquelier, J. Rodríguez-Carvajal, E. Elkaim, J.-P. Lauriat, and J. L. Martínez, Chem. Mater. **11**, 3629 (1999).
[6]I. Kornev, M. Bichurin, J.-P. Rivera, S. Gentil, H. Schmid, A. G. M. Jansen, and P. Wyder, Phys. Rev. B **62**, 12247 (2000).
[7]N. Recham, J.-N. Chotard, J.-C. Jumas, L. Laffont, M. Armand, and J.-M. Tarascon, Chem. Mater. **22**, 1142 (2010).
[8]P. Barpanda, K. Djellab, N. Recham, M. Armand, and J.-M. Tarascon, J. Mater. Chem. **21**, 10143 (2011).
[9]M. Ati, B. C. Melot, G. Rousse, J.-N. Chotard, P. Barpanda, and J.-M. Tarascon, Angew. Chem. Int. Ed. **50**, 10574 (2011).
[10]R. Tripathi, T. N. Ramesh, B. L. Ellis, and L. F. Nazar, Angew. Chem. Int. Ed. **49**, 8738 (2010).
[11]P. Barpanda, M. Ati, B. C. Melot, G. Rousse, J.-N. Chotard, M.-L. Doublet, M. T. Sougrati, S. A. Corr, J.-C. Jumas, and J.-M. Tarascon, Nat. Mater. **10**, 772 (2011).
[12]M. Ati, B. C. Melot, J.-N. Chotard, G. Rousse, M. Reynaud, and J.-M. Tarascon, Electrochem. Commun. **13**, 1280 (2011).
[13]B. C. Melot, G. Rousse, J.-N. Chotard, M. Ati, J. Rodríguez-Carvajal, M. C. Kemei, and J.-M. Tarascon, Chem. Mater. **23**, 2922 (2011).
[14]T. Mueller, G. Hautier, A. Jain, and G. Ceder, Chem. Mater. **23**, 2854 (2011).
[15]M. Reynaud, P. Barpanda, G. Rousse, J.-N. Chotard, B. C. Melot, N. Recham, and J.-M. Tarascon, Solid State Sci. **14**, 15 (2012).
[16]M. Ati, L. Dupont, N. Recham, J.-N. Chotard, W. T. Walker, C. Davoisne, P. Barpanda, V. Sarou-Kanian, M. Armand, and J.-M. Tarascon, Chem. Mater. **22**, 4062 (2010).
[17]J. Rodríguez-Carvajal, Phys. B **192**, 55 (1993).
[18]H. M. Rietveld, J. Appl. Crystallogr. **2**, 65 (1969).
[19]I. D. Brown and D. Altermatt, Acta Crystallogr., Sect. B, Struct. Sci. **41**, 244 (1985).
[20]E. F. Bertaut, J. Phys. Colloques **32**, C1 (1971).
[21]J. Rodríguez-Carvajal, BASIREPS—A program for calculating non-normalized basis functions of the irreductible representations of the little group G_k for atom properties in a crystal, Laboratoire Leon Brillouin, CEA Saclay, Gif sur Yvette, France, 2004.
[22]P. Barpanda, J.-N. Chotard, N. Recham, C. Delacourt, M. Ati, L. Dupont, M. Armand, and J.-M. Tarascon, Inorg. Chem. **49**, 7401 (2010).
[23]R. D. Shannon, Acta Crystallogr., Sect. A, Cryst. Phys. Diffr. Theor. Gen. Crystallogr. **32**, 751 (1976).
[24]M. C. Day and J. Selbin, *Theoretical Inorganic Chemistry*, 2nd ed. (Reinhold, New York, 1960).
[25]J. B. Goodenough, Phys. Rev. **117**, 1442 (1960).
[26]J. Kanamori, J. Phys. Chem. Solids **10**, 87 (1959).
[27]P. W. Anderson, Phys. Rev. **79**, 350 (1950).
[28]G. Rousse, J. Rodríguez-Carvajal, C. Wurm, and C. Masquelier, Chem. Mater. **13**, 4527 (2001).
[29]G. Rousse, J. Rodríguez-Carvajal, C. Wurm, and C. Masquelier, Appl. Phys. A. **74**, S704 (2002).
[30]G. Rousse, J. Rodríguez-Carvajal, S. Patoux, and C. Masquelier, Chem. Mater. **15**, 4082 (2003).
[31]B. C. Melot, A. Goldman, L. E. Darago, J. D. Furman, E. E. Rodriguez, and R. Seshadri, J. Phys. Condens. Matter **22**, 506003 (2010).
[32]B. C. Melot, B. Paden, R. Seshadri, E. Suard, G. Nénert, A. Dixit, and G. Lawes, Phys. Rev. B **82**, 014411 (2010).
[33]C. F. Smura, D. R. Parker, M. Zbiri, M. R. Johnson, Z. A. Gál, and S. J. Clarke, J. Am. Chem. Soc. **133**, 2691 (2011).
[34]E. O. Wollan and W. C. Koehler, Phys. Rev. **100**, 545 (1955).
[35]J. C. Slonczewski, Phys. Rev. **110**, 1341 (1958).
[36]B. C. Melot, J.-N. Chotard, G. Rousse, M. Ati, M. Reynaud, and J.-M. Tarascon, Inorg. Chem. **50**, 7662 (2011).
[37]O. Mentre, F. Bouree, J. Rodríguez-Carvajal, A. El Jazouli, N. El Khayati, and E. M. Ketatni, J. Phys. Condens. Matter **20**, 415211 (2008).
[38]G. Rousse, J. Rodríguez-Carvajal, C. Wurm, and C. Masquelier, Solid State Sciences **4**, 973 (2002).
[39]J. Rodríguez-Carvajal, Programs SIMBO, ENERMAG are available within the examples of the CrysFML repository at [http://forge.ill.eu/projects/crysfml/repository].